HYPERSPECTRAL TARGET DETECTION AND APPLICATION TO LOW ABUNDANCE SERPENTINE MAPPING. X. Wu[1, 2], J. F. Mustard[2], X. Zhang[1], J. D. Tarnas[2]. Institute of Remote Sensing and Digital Earth, CAS, Beijing, 100101 (wuxing@radi.ac.cn), [2]Dept. of Earth, Environmental, and Planetary Sciences, Brown University, RI, 02912.

Introduction: Mineral detection on Mars through hyperspectral remote sensing is of prime importance for understanding the composition of its surface and subsurface. Typically regions of interest are identified by spectral parameters, and spectra from these regions are then intensively analyzed in the context of laboratory spectra of known minerals [1, 2]. While effective, this approach is time consuming and subject to error or omission. Furthermore, it is not suitable for large scale mineral mapping. Hydrated mineral outcrops are usually small and/or subpixel level at typical spacecraft instrument spatial resolutions. Target detection (TD) focuses on distinguishing small and rare target pixels from various background pixels with *a priori* knowledge of target spectra [3]. Thus, TD is suitable for mapping low occurrence but scientifically valuable minerals. In this work, a new method to detect the presence and location of target minerals at low abundances has been developed and applied to a laboratory visible and near-infrared (VNIR) hyperspectral image (HSI) containing Mars global simulant (MGS) [4] and serpentine mixtures.

Method: In this work, a new mineral detection method that joins the Hapke model [5] and spatially adaptive sparse representation-based (STD) is proposed. The reflectance of each pixel is first converted to single scattering albedo (SSA) using the Hapke model, after which the spatial adaptive STD (SASTD) is applied to the SSA data in three steps:

1) *Single scattering albedo (SSA) retrieval.* Due to the mineral particles being in close contact with each other, complex interactions introduce nonlinearities in reflectance. SSA is linearly additive in visible and infrared wavelengths [5]. The purpose of this step is to convert the reflectance to SSA. Consequently, the linear TD method can be implemented on SSA data.

2) *Background and target dictionaries construction.* The target dictionary is constructed using *a priori* knowledge of target spectra, while the background dictionary is generated locally through a dual window. However, target pixels may fall into the background due to improper window size settings or the sliding window process. We propose an iterative background purification strategy to remove the potential target pixels in the background dictionary.

3) *Spectral reconstruction and target detection.* A spatially adaptive STD [6] is adopted in this work, which incorporates spatial information into TD.

We compare the proposed method with several traditional and state-of-the-art TD algorithms: (1) constrained energy minimization (CEM) [7]; (2) matched filter (MF) [3]; (3) sparse representation-based detector (STD) [8]; (4) SASTD [6]. The performance is assessed with metrics: 1) a detection map 2) receiver operating characteristic (ROC) curve and 3) area under curve (AUC) value. The ROC curve illustrates the relationship between the detection probability P_d and the false alarm rate P_f at a series of thresholds. P_d and P_f are defined as [9]

$$P_d = \frac{N_d}{N_T} \text{ and } P_f = \frac{N_{miss}}{N_{all}} \quad (1)$$

where N_d is the number of detected target pixels at a certain threshold; N_T denotes the number of total target pixels in the image; N_{miss} represents the number of background pixels mistaken as targets; N_{all} is the number of total pixels in the image.

Data: We employ the experimental design described by [10]. Powders of serpentine and a Mars global simulant [5] (MGS-1) were mixed by six mass proportions. The serpentine abundance are 0%, 1%, 2.5%, 5%, 10% and 100%, respectively. MGS-1 is an excellent physical and spectroscopic analog to the global basaltic soil [5]. The samples were measured at Brown University using a Headwall imaging spectrometer. The spectral sampling interval is 8.98 nm and the instantaneous field of view (IFOV) is 1.36 mrad. The data were converted from the digital number (DN) to reflectance, more details about the data acquisition can be found in [10]. Figure 1 shows the reflective spectra and corresponding SSA of the mixtures. Each curve is an average of 5x5 pixels.

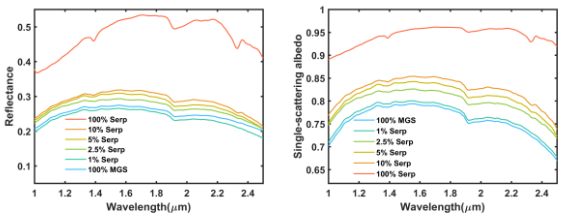

Figure 1. Reflectance and SSA curves of six sample trays in the Headwall dataset. (left) Reflectance of each sample tray. (right) SSAs of each sample trays.

Results: The two-dimensional detection maps of all detectors are presented in Figure 2. Each grid contains 11x11 pixels. For a fair comparison, all the detection results are normalized to 0~1. The colorbar indicates the confidence of a pixel to be a target. The red color represents the pixel is likely to be a target (serpentine), while the blue color shows the pixel is likely to be a background (MGS). We only show the detection map with the SSA data due to the limit of the page. The detection value contrast of different abundance mixtures in the sparse representation-based methods is higher than that of other detection methods. By introducing the spatial constraint, our mapping results are more homogeneous than the others. The detection maps on the reflectance data have the same trend but which only definitely identify the 100% and 10% serpentine.

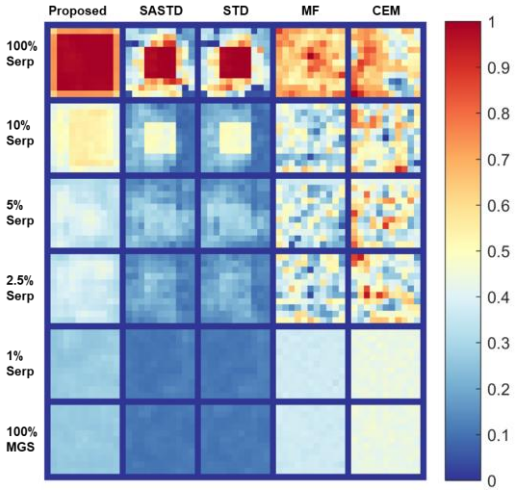

Figure 2. Detection results using Headwall data. The red color represents the pixel is likely to be a target while the blue color is likely to be a background.

A good detection ROC curve should lie near to the upper left. With these Headwall data, the ROC curves of sparse representation-based detectors are above those of traditional detectors CEM, and MF (Figure 3). For the SSA dataset, the ROC curve of the proposed method broadly encloses those of other detectors, especially when P_f ranges from 0.005 to 1. It is observed that the ROC curve of each detector for the reflectance data is below that of its SSA's version, which makes clear that SSA is more suitable for mineral detection.

The AUC values for the different detectors are shown in Table 1. The best results are labeled in bold. In reflectance data, the AUC value obtained by SASTD is improved from 0.7469 to 0.7799 by purifying the background dictionary. In SSA space, the proposed method achieves the best AUC value of 0.8938.

We also evaluated the detection performance of the proposed approach on each serpentine tray. As shown in Figure 4, the AUC values are above 0.86 except for 1% serpentine. The AUC value for 5% serpentine is smaller than for 2.5% serpentine due to structured noise and powder inhomogeneities within 5% serpentine region.

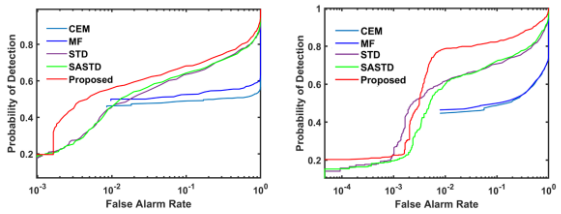

Figure 3. ROC curves of all detectors on the Headwall dataset. (left) reflectance dataset. (right) SSA dataset.

Table 1. AUC values for the different detectors with the two datasets

Algorithm	Dataset	
	Reflectance	SSA
CEM	0.5090	0.5924
MF	0.5584	0.5971
STD	0.7455	0.8025
SASTD	0.7469	0.8121
proposed	**0.7799**	**0.8938**

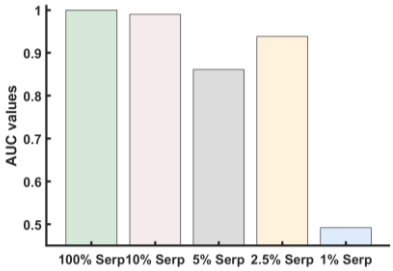

Figure 4. AUC values of the proposed algorithm on each serpentine tray.

Conclusions: 1) The proposed method achieves the best detection performance. 2) As shown in Figure 4, our method is able to detect low abundance serpentine (above 2.5%) in the binary mixtures. The 1% serpentine is beyond the detection ability since the signal is too weak. How to coordinate laboratory and orbital detections is the focus of our future research.

References: [1] Mustard et al. (2008) *Nature*, 454, 305-309. [2] Carter et al. (2013) *JGR*, 118, 831-858. [3] Manolakis. (2002) *GRSM*, 19, 29-43. [4] Cannon et al. (2019) *Icarus*, 317, 470-478. [5] Hapke. (1983) *JGR*, 86, 3039-3054. [6] Zhang et al. (2017) *GRSL*, 14, 1923–1927. [7] Farrand et al. (1997) *RSE*, 59, 64-76. [8] Chen et al. (2011) *JSTSP*, 5, 629-640. [9] Zou et al. (2016) *TGRS*, 54, 330-342. [10] Das et al. (2020) *51th LPSC*.